12. Nakamura, R. *et al.* Spatial scale of high-speed flows in the plasma sheet observed by Cluster. *Geophys. Res. Lett.* **31**, doi:10.1029/2004GL019558 (2004).
13. Louarn, P. *et al.* Cluster observations of complex 3D magnetic structures at the magnetopause. *Geophys. Res. Lett.* **31**, doi:10.1029/2004GL020625 (2004).
14. Phan, T. D. *et al.* Extended magnetic reconnection at the Earth's magnetopause from detection of bi-directional jets. *Nature* **404**, 848–850 (2000).
15. Fuselier, S. A. *et al.* Cusp aurora dependence on IMF B_y. *J. Geophys. Res.* **107**, 1111, doi:10.1029/2001JA900165 (2002).
16. Pinnock, M. *et al.* The location and rate of dayside reconnection during an interval of southward interplanetary magnetic field. *Ann. Geophys.* **21**, 1467–1482 (2003).
17. Gosling, J. T. *et al.* Direct evidence for magnetic reconnection in the solar wind near 1AU. *J. Geophys. Res.* **100**, doi:10.1029/2004JA010809 (2005).
18. Gosling, J. T. *et al.* Magnetic disconnection from the Sun: Observations of a reconnection exhaust in the solar wind at the heliospheric current sheet. *Geophys. Res. Lett.* **32**, doi:10.1029/2005GL022406 (2005).
19. Petschek, H. E. in *AAS-NASA Symp. on the Physics of Solar Flares* (28–30 October 1963, Goddard Space Flight Centre, Greenbelt, Maryland) (ed. Hess, W. N.) 425–437 (NASA Spec. Publ. SP-50, NASA Science and Technical Information Division, Washington DC, 1964).
20. Sonnerup, B. U. Ö. & Cahill, L. J. Jr Magnetopause structure and attitude from Explorer 12 observations. *J. Geophys. Res.* **72**, 171–183 (1967).
21. Sonnerup, B. U. Ö. Magnetopause reconnection rate. *J. Geophys. Res.* **79**, 1546–1549 (1974).
22. Gosling, J. T. *et al.* Evidence for quasi-stationary reconnection at the dayside magnetopause. *J. Geophys. Res.* **87**, 2147–2158 (1982).
23. Frey, H. *et al.* Continuous magnetic reconnection at Earth's magnetopause. *Nature* **426**, 533–537 (2003).
24. Phan, T. D. *et al.* Cluster observations of continuous reconnection at the magnetopause under steady interplanetary magnetic field conditions. *Ann. Geophys.* **22**, 2355–2367 (2004).
25. Paschmann, G. *et al.* The magnetopause for large magnetic shear: AMPTE/IRM observations. *J. Geophys. Res.* **91**, 11099–11115 (1986).
26. Hudson, P. D. Discontinuities in an anisotropic plasma and their identification in the solar wind. *Planet. Space Sci.* **18**, 1611–1622 (1970).

Acknowledgements Wind, ACE and Cluster research in the US is supported by NASA. Cluster research in France and the UK is supported by CNES and PPARC.

Author Information Reprints and permissions information is available at npg.nature.com/reprintsandpermissions. The authors declare no competing financial interests. Correspondence and requests for materials should be addressed to T.D.P. (phan@ssl.berkeley.edu).

LETTERS

A semiconductor source of triggered entangled photon pairs

R. M. Stevenson[1], R. J. Young[1,2], P. Atkinson[2], K. Cooper[2], D. A. Ritchie[2] & A. J. Shields[1]

Entangled photon pairs are an important resource in quantum optics[1], and are essential for quantum information[2] applications such as quantum key distribution[3,4] and controlled quantum logic operations[5]. The radiative decay of biexcitons—that is, states consisting of two bound electron–hole pairs—in a quantum dot has been proposed as a source of triggered polarization-entangled photon pairs[6]. To date, however, experiments have indicated that a splitting of the intermediate exciton energy yields only classically correlated emission[7–9]. Here we demonstrate triggered photon pair emission from single quantum dots suggestive of polarization entanglement. We achieve this by tuning the splitting to zero, through either application of an in-plane magnetic field or careful control of growth conditions. Entangled photon pairs generated 'on demand' have significant fundamental advantages over other schemes[10–13], which can suffer from multiple pair emission, or require post-selection techniques or the use of photon-number discriminating detectors. Furthermore, control over the pair generation time is essential for scaling many quantum information schemes beyond a few gates. Our results suggest that a triggered entangled photon pair source could be implemented by a simple semiconductor light-emitting diode[14].

The most widely used methods for generating entangled photon pairs are nonlinear optical processes, such as parametric down conversion[10,12], which produce a probabilistic number of pairs per excitation cycle. Existing demonstrations of entangled photons in semiconductor systems also do not produce individual entangled photon pairs on demand. For the nonlinear process involved in bulk CuCl, the number of pairs emitted follows poissonian statistics[15]. For entangled photon pairs created by the probabilistic interference of indistinguishable photons from a single quantum dot[16], post selection is required to reject the majority of photons which are not entangled[13], and even for the idealized case only 50% of the photons are entangled. Thus the realization of a quantum dot source that emits no more than one entangled photon pair per excitation cycle is fundamentally different to the demonstrations described above. It is perhaps more closely related to generation of entangled photons in single atoms[17], of which a quantum dot may be considered the semiconductor analogue. Another appealing feature is that after the first photon is emitted, the proposed single quantum dot system resides in an entangled photon-exciton state, opening up the possibility of implementing quantum logic operations in the solid state as well as photonic domains.

The radiative decay of the biexciton state (XX) in a quantum dot emits a pair of photons, with polarization determined by the spin of the intermediate exciton state (X). In an ideal quantum dot with degenerate X states, the polarization of the XX photon is predicted to be entangled with that of the X photon, forming the state $(|H_{XX}H_X> + |V_{XX}V_X>)/\sqrt{2}$, where H and V denote the polarization of the XX and X photons[6].

In real quantum dots, the polarization of a photon can also be determined by its energy, due to splitting of the intermediate exciton state, shown schematically in Fig. 1. The splitting exists because of in-plane asymmetries of structural properties of the quantum dot, such as elongation and strain[18,19], and provides 'which path' information, preventing polarization entanglement of the emission. The key to the generation of entangled photon pairs in a quantum dot is therefore the reduction of the exciton polarization splitting to zero. Here we describe how we were able to carefully select unsplit quantum dots, or alternatively apply an in-plane magnetic field to tune the splitting to zero.

By characterizing the exciton polarization splitting of a large number of InAs/GaAs quantum dots from samples grown under different conditions, we found the splitting to be least for relatively

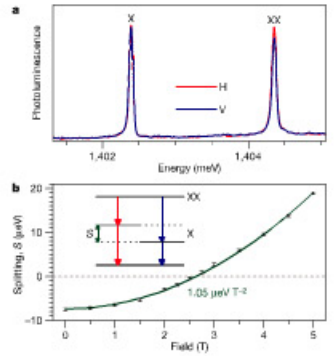

Figure 1 | Polarized photoluminescence spectra from single quantum dots. **a**, Vertically (blue) and horizontally (red) polarized photoluminescence for a single quantum dot with small polarization splitting. The features correspond to emission by the exciton (X) and biexciton (XX) state. **b**, Polarization splitting, S, as a function of in-plane magnetic field for a single dot with 'inverted' S at 0 T. The green line shows a quadratic fit to the data with a coefficient of 1.05 μeV T^{-2}. Inset shows the level diagram of the radiative decay of the biexciton state. The competing two photon decay paths are distinguished only by the polarization of the photons, indicated by the arrow colour, and the splitting, S, of the intermediate exciton level. Error bars span two standard deviations from the fitted line.

[1]Toshiba Research Europe Limited, 260 Cambridge Science Park, Cambridge CB4 0WE, UK. [2]Cavendish Laboratory, University of Cambridge, Madingley Road, Cambridge CB3 0HE, UK.

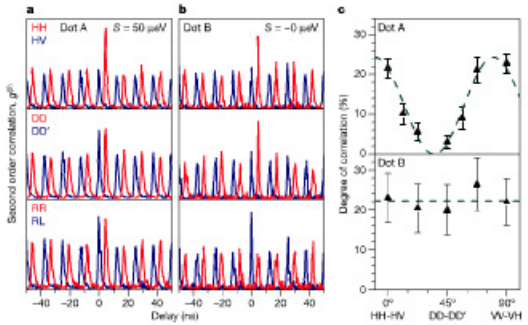

Figure 2 | Second order cross correlation of biexciton with exciton photons from conventional and degenerate single quantum dots. **a**, **b**, Cross correlation for a reference dot A with 50 μeV polarization splitting (**a**), and a degenerate dot B (**b**). Correlations measured for photons of the same polarization are shown in red, and for orthogonal polarization in blue. The red histograms are time shifted to allow easier comparison to the blue. The top, middle and bottom panels represent correlations measured in the rectilinear, diagonal and circular bases, respectively. **c**, The degree of linear correlation is plotted as a function of the basis angle. Error bars span two standard deviations. H, horizontal; V, vertical; D, diagonal; D', orthodiagonal; R, right; L, left.

small dots emitting at ~1.4 eV, in which the electron and hole wavefunctions are most symmetric[20]. Figure 1a plots polarized photoluminescence spectra at ~10 K, recorded for a typical dot showing near-zero splitting. The biexciton photon emission energy is 1.96 meV higher than the exciton photon emission energy, which is quite typical for this kind of small quantum dot[21,22]. The energy difference, due to the Coulomb interaction, allows simple wavelength selective separation of the two photons in the pair, which is not possible in most schemes for entangled photon generation that require the photons to have the same energy. No polarization splitting can be resolved by eye between the horizontally and vertically polarized components of the emission. The fitted central wavelengths of all lines were used to determine the average polarization splitting for the exciton and biexciton. The resulting measured exciton splitting was found to be 1.1 ± 0.5 μeV, within the projected homogeneous linewidth of ~1.5 μeV.

The samples show considerable difference in the magnitude and sign of splitting from dot to dot, owing to variations in dot size, shape and composition. However, we have found that the polarization splitting of many dots can be tuned to zero by applying an in-plane magnetic field. These dots are identified by the negative sign of their splitting, using the sign convention that the splitting equals the energy of the horizontally polarized exciton minus that of the vertically polarized one. The tuning of the polarization splitting of an example dot by magnetic field is shown in Fig. 1b. The splitting varies approximately quadratically with magnetic field from −7.6 ± 0.5 μeV to +19.3 ± 0.5 μeV. Most importantly, the splitting can be tuned to approximately zero for an applied field of 2.5 ± 0.1 T. As we shall show later, this provides a way to turn on entangled photon generation by the quantum dot.

Polarization dependent two photon correlations were measured as detailed in the Methods section. Figure 2a shows the second order cross correlation between the XX and X photon emitted by a reference dot A, for which the exciton splitting was 49.9 ± 0.5 μeV. The polarization correlated traces shown in red are artificially time shifted relative to the polarization anti-correlated traces shown in blue, to aid comparison. The average total number of counts in the peaks at zero delay is larger than the average number of counts in the other peaks. This is due to the greater probability of detecting an X photon in the same period that an XX photon was detected. The degree of enhancement is dependent on the excitation efficiency, which is the same for each pair of traces recorded simultaneously, allowing direct comparison. The three panels represent correlations measured in the rectilinear, diagonal and circular bases, and were measured using a half wave plate set at 0° and 22.5°, and a quarter wave plate set at 45°, placed directly after the collection lens. The top panel shows a much higher probability of generating a pair of photons with the same rectilinear polarization. Detection of oppositely polarized photon pairs is not fully suppressed owing to contribution from background light and exciton dephasing, discussed later in detail. However, no polarization correlation at all is observed in the diagonal or circular bases, demonstrated by the middle and bottom panels. The photon pairs emitted by the reference dot are therefore only classically polarization correlated as observed previously[7–9], and not entangled.

The correlation experiment was repeated for dot B, which has approximately zero splitting. The results are shown in Fig. 2b. A similar degree of rectilinear polarization correlation is observed as for the reference dot A, and indeed all dots measured. However, strong diagonal polarization correlation is additionally observed, and remarkably also strong circular polarization anti-correlation. This is consistent with expected results for entangled photon emission from a single quantum dot.

A well known property of entangled photon pairs is that the degree of correlation does not depend on the absolute orientation of the photons, but only the difference in the angle between them[12]. The degree of linear correlation was measured as a function of the linear polarization basis angle by rotating the half wave plate, which has no effect on the difference in polarization detection angles, which was effectively parallel. The results are shown in Fig. 2c. For the reference dot A, the correlation fits well to sinusoidal behaviour between zero and a maximum of 0.243 ± 0.012, as expected for classically linearly polarization correlated photon pairs. In stark contrast, the degree of correlation for the degenerate dot B is independent of the orientation of the measurement basis within experimental error, as expected for polarization entangled photon pairs. The average degree of correlation is found to be 0.222 ± 0.028, similar to the maximum of the reference dot. Again this is what is expected for entangled photon

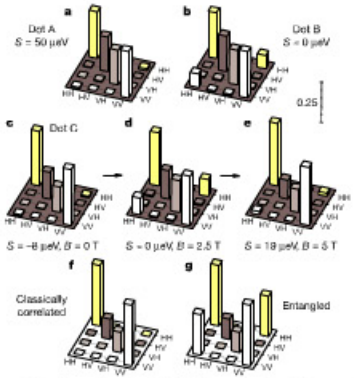

Figure 3 | Density matrices for the biexciton–exciton two-photon cascade from conventional and degenerate quantum dots. **a**–**e**, Real parts of measured density matrices corresponding to reference dot A with polarization splitting, $S = 50\,\mu eV$ (**a**), dot B with $S \approx 0\,\mu eV$ at 0 T (**b**), and dot C, with S tuned by the magnetic field to be $-8\,\mu eV$ (**c**), $0\,\mu eV$ (**d**) and $19\,\mu eV$ (**e**). The imaginary components are not shown, and were zero within experimental error. Density matrices **b** and **d** feature strong outer off diagonal elements associated with entangled photon pair states, which are not present in the reference case (**a**). **f**, **g**, Density matrices representing the predicted state for ideal classically correlated (**f**) and entangled (**g**) photon pairs, including 50% contribution from uncorrelated background light.

pairs, in contrast to the case of classically correlated photon pairs emitting into random bases, for which the average degree of correlation should be less by a factor of 2.

To fully measure the two photon polarization state, a quantum state tomography scheme was used[23,24]. The procedure, detailed in the Methods section, constructs the two photon polarization density matrix from a linear combination of cross correlation measurements using 16 different polarization combinations.

The real component of the two photon polarization density matrix for the reference dot A is shown in Fig. 3a. The stronger elements all lie on the diagonal, with the strongest outer elements indicating polarization correlated emission. The inner diagonal components are due to uncorrelated photon pair emission, from background counts and dephasing of the exciton state. The form of this density matrix is consistent with imperfect polarization correlated photon pair emission seen previously[7–9], and illustrated by the example density matrix of Fig. 3f. The density matrix for the degenerate dot shown in Fig. 3b has similar diagonal elements, but now shows significant outer, off diagonal elements. This is a feature associated with polarization entangled photon pairs, illustrated by the predicted density matrix of Fig. 3g.

A similar density matrix is obtained for dot C, tuned to zero splitting by magnetic field, as shown in Fig. 3d. This again suggests that the photon pair emission has entangled character. When the field is increased to 5 T, the splitting increases to 19 μeV, and the corresponding density matrix measured is shown in Fig. 3e. As expected, the off diagonal elements are suppressed, and the dot reverts to emitting polarization correlated photon pairs. A similar result is found if the field is reduced to 0 T, where the splitting is −8 μeV as shown in Fig. 3c. The imaginary components of the density matrices were all found to be zero with experimental error, in agreement with predictions.

The measurements presented above clearly suggest that dots with small exciton splitting emit entangled photons. We now discuss the factors limiting the degree of entanglement. In spectroscopy, our measurements show that the background due to dark counts and emission from layers other than the dot contributes on average 49% of the coincidence counts; this is unusually large owing to the proximity of the dot to the wetting layer, which is necessary to select dots with zero splitting. If we correct our measurements by removing the projected number of background counts from the correlation data, the density matrices of the degenerate and magnetically tuned dots more closely resemble the ideal entangled case, and the largest eigenvalues are 0.48 ± 0.08 and 0.58 ± 0.04, respectively. The latter, for which the splitting is minimal, violates the 0.5 limit for classical correlation in an unpolarized source[25]. The remaining deviation from ideal behaviour is attributed to scattering between the two intermediate exciton spin states[7,9]. From previous publications where strong background and entanglement were not present, we estimate an exciton scattering time similar to the ~1 ns radiative lifetime. This yields a maximum possible eigenvalue of 0.63, in rough agreement with these measurements.

This suggests that the degree of entanglement may be increased by resonant optical[10,26] or electrical[8] excitation in order to increase the scattering time, or by reducing the radiative lifetime through Purcell enhancement[27,28], or by using dots with larger oscillator strength such as those formed by interface fluctuations[18]. Such improvements could lead to the realization of a semiconductor source of triggered entangled photon pairs that would be robust and compact, and allow electrical injection of the carriers[14].

METHODS

Sample fabrication and characterization. Samples containing a low density layer of InAs quantum dots (~1.6 monolayers thick) were grown by molecular beam epitaxy. A GaAs λ cavity containing the dot layer was surrounded by AlAs/GaAs distributed Bragg reflectors, with 14 (2) repeats in the bottom (top) mirror, to increase light collection efficiency. A metal shadow mask containing apertures of ~2 μm diameter was fabricated to isolate the emission of individual dots. Samples with a range of InAs thicknesses differing by up to ~2% were characterized in a standard micro photoluminescence system operating at ~10 K. Optical excitation was provided by ~100-ps pulses from a 635-nm laser diode operating at 80 MHz. The emission lines are inhomogeneously broadened by charge fluctuations to ~50 μeV, a consequence of the non-resonant excitation scheme[29]. Horizontally ([110]) and vertically ([1−10]) polarized exciton and biexciton emission was fitted with lorentzian line shapes to locate the centre energy of each transition. The exciton level splitting can be determined both from the difference between the horizontally and vertically polarized exciton or biexciton photons. Taking the average of these two values removed systematic error associated with changing the polarization optics, and the splitting S was measured with an estimated precision of ~0.5 μeV.

Selection of suitable dots. By measuring the splitting of 200 quantum dots, a relationship of decreasing splitting with increasing emission energy was found[29]. For dots emitting at ~1.4 eV, the splitting was ~0 ± 10 μeV. Thus quantum dots with splitting less than the homogeneous linewidth of ~1.5 μeV were selected first by identifying dots emitting close to 1.4 eV, then measuring their splitting. For dots emitting >1.4 eV, the splitting was inverted, and the lowest energy exciton line is horizontally polarized. For these dots, the configuration of the exchange energies and g-factors allows reduction of the splitting with an applied in-plane magnetic field, driven by partial mixing of optically active and inactive exciton states[30]. Thus dots suitable for tuning to zero splitting are conveniently identified by their emission energy. The proportion of dots that have, or can be tuned to, zero splitting is ~30%, which could be improved by better growth control. The proportion of suitably isolated single dots could be improved by fabrication of smaller microstructures.

Photon pair counting. Quantum dots were optically excited, with the power adjusted to give optimum photon pair detection rate to background ratio. At this power, the biexciton intensity is around half that of the exciton. A 50/50 beam splitter divided the emission into two spectrometers, set to transmit at the XX and X photon energies respectively, with ~0.5 meV bandwidth. Polarizing beam splitters were placed after the spectrometers, and three single photon detectors

were used to measure the vertically polarized XX photons, and horizontally and vertically polarized X photons. The time between detection of XX photons and X photons was measured by a time interval analyser.

Photons can be counted over a number of hours by compensating for fluctuations in excitation and detection efficiency over time. This is achieved by determining the degree of correlation from the ratio of the two correlations measured simultaneously, each normalized by the number of pairs detected in different laser cycles.

The approach is valid for unpolarized sources, and unpolarizing transmission of the light collection system up to the wave plates. Our system satisfies these requirements, as the emission was unpolarized within error, and the transmission was only weakly polarizing. For the results of Fig. 2, a single half or quarter wave plate was inserted directly after the collection lens to select the measurement basis for the exciton and biexciton photons simultaneously, and the transmission was zero within experimental error. For the measurements of Fig. 3, a quarter wave and half wave plate was used before each spectrometer to select the polarization detection basis for the exciton and biexciton independently, and the transmission was only ~10% polarizing. The total number of coincident pairs detected over the course of an experiment is typically up to 1,000, which dictates the measurement errors.

Quantum tomography analysis. The probability that a photon pair is detected with a selected polarization combination was determined experimentally from pairs of two photon correlations measured simultaneously. 16 such measurements were used to construct each two photon density matrix, using the polarization combinations and methods of ref. 24. The density matrix fully describes the two-photon quantum state, and thus can be used to test for entanglement. The test we chose is that of the largest eigenvalue, which is a general test that makes no assumption about the nature of the entangled state, in contrast to a Bell inequality, for which violation is maximal when the entangled state corresponds to that for which the polarization measurement bases were chosen. For an unpolarized classical source, the probability that a photon pair exists in any given polarization state cannot exceed 0.5, therefore an eigenvalue >0.5 signifies the presence of entanglement.

Received 28 July; accepted 16 November 2005.

1. Walls, D. F. & Milburn, G. J. *Quantum Optics* (Springer, Berlin, 1994).
2. Bouwmeester, D., Ekert, A. K. & Zeilinger, A. *The Physics of Quantum Information* (Springer, Berlin, 2000).
3. Ekert, A. K. Quantum cryptography based on Bell's theorem. *Phys. Rev. Lett.* **67**, 661–663 (1991).
4. Gisin, N., Ribordy, G., Tittel, W. & Zbinden, H. Quantum cryptography. *Rev. Mod. Phys.* **74**, 145–195 (2002).
5. Knill, E., Laflamme, R. & Milburn, G. J. A scheme for efficient quantum computation with linear optics. *Nature* **409**, 46–52 (2001).
6. Benson, O., Santori, C., Pelton, M. & Yamamoto, Y. Regulated and entangled photons from a single quantum dot. *Phys. Rev. Lett.* **84**, 2513–2516 (2000).
7. Stevenson, R. M. *et al.* Quantum dots as a photon source for passive quantum key encoding. *Phys. Rev. B* **66**, 081302 (2002).
8. Santori, C., Fattal, D., Pelton, M., Solomon, G. S. & Yamamoto, Y. Polarization-correlated photon pairs from a single quantum dot. *Phys. Rev. B* **66**, 045308 (2002).
9. Ulrich, S. M., Strauf, S., Michler, P., Bacher, G. & Forchel, A. Triggered polarization-correlated photon pairs from a single CdSe quantum dot. *Appl. Phys. Lett.* **83**, 1848–1850 (2003).
10. Shih, Y. H. & Alley, C. O. New type of Einstein-Podolsky-Rosen-Bohm experiment using pairs of light quanta produced by optical parametric down conversion. *Phys. Rev. Lett.* **61**, 2921–2924 (1988).
11. Ou, Z. Y. & Mandel, L. Violation of Bell's inequality and classical probability in a two-photon correlation experiment. *Phys. Rev. Lett.* **61**, 50–53 (1988).
12. Kiess, T. E., Shih, Y. H., Sergienko, A. V. & Alley, C. O. Einstein-Podolsky-Rosen-Bohm experiment using pairs of light quanta produced by type-II parametric down-conversion. *Phys. Rev. Lett.* **71**, 3893–3897 (1993).
13. Fattal, D. *et al.* Entanglement formation and violation of Bell's inequality with a semiconductor single photon source. *Phys. Rev. Lett.* **92**, 037903 (2004).
14. Yuan, Z. *et al.* Electrically driven single-photon source. *Science* **295**, 102–105 (2002).
15. Edamatsu, K., Oohata, G., Shimizu, R. & Itoh, T. Generation of ultraviolet entangled photons in a semiconductor. *Nature* **431**, 167–170 (2004).
16. Santori, C., Fattal, D., Vučković, J., Solomon, G. S. & Yamamoto, Y. Indistinguishable photons from a single-photon device. *Nature* **419**, 594–597 (2002).
17. Aspect, A., Grangier, P. & Roger, G. Experimental realization of Einstein-Podolsky-Rosen-Bohm Gedankenexperiment: A new violation of Bell's inequalities. *Phys. Rev. Lett.* **49**, 91–94 (1982).
18. Gammon, D., Snow, E. S., Shanabrook, B. V., Katzer, D. S. & Park, D. Fine structure splitting in the optical spectra of single GaAs quantum dots. *Phys. Rev. Lett.* **76**, 3005–3008 (1996).
19. Bimberg, D., Grundmann, M. & Ledentsov, N. N. *Quantum Dot Heterostructures* (Wiley, Chichester, 1999).
20. Young, R. J. *et al.* Inversion of exciton level splitting in quantum dots. *Phys. Rev. B* **72**, 113305 (2005).
21. Thompson, R. M. *et al.* Single-photon emission from exciton complexes in individual quantum dots. *Phys. Rev. B* **64**, 201302 (2001).
22. Rodt, S. *et al.* Repulsive exciton-exciton interaction in quantum dots. *Phys. Rev. B* **68**, 035331 (2003).
23. White, A. G., James, D. F. V., Eberhard, P. H. & Kwiat, P. G. Nonmaximally entangled states: Production, characterization, and utilization. *Phys. Rev. Lett.* **83**, 3103–3107 (1999).
24. James, D. F. V., Kwiat, P. G., Munro, W. J. & White, A. G. Measurement of qubits. *Phys. Rev. A* **64**, 052312 (2001).
25. Kwiat, P. G., Barraza-Lopez, S., Stefanov, A. & Gisin, N. Experimental entanglement distillation and 'hidden' non-locality. *Nature* **409**, 1014–1017 (2001).
26. Santori, C., Pelton, M., Solomon, G., Dale, Y. & Yamamoto, Y. Triggered single photons from a quantum dot. *Phys. Rev. Lett.* **86**, 1502–1505 (2001).
27. Pelton, M. *et al.* Efficient source of single photons: A single quantum dot in a micropost microcavity. *Phys. Rev. Lett.* **89**, 233602 (2002).
28. Bennett, A. J., Unitt, D. C., Atkinson, P., Ritchie, D. & Shields, A. J. High performance single photon sources from photolithographically defined pillar microcavities. *Opt. Express* **13**, 50–55 (2005).
29. Bayer, M. & Forchel, A. Temperature dependence of the exciton homogeneous linewidth in $In_{0.60}Ga_{0.40}As/GaAs$ self-assembled quantum dots. *Phys. Rev. B* **65**, 041308 (2002).
30. Stevenson, R. M. *et al.* Magnetic-field-induced reduction of the exciton polarization splitting in InAs quantum dots. *Phys. Rev. B* (in the press).

Acknowledgements We acknowledge continued support from M. Pepper. This work was partially funded by the EU projects RAMBOQ, QAP and SANDiE, and by the EPSRC through the IRC for Quantum Information Processing.

 Correspondence and requests for materials should be addressed to R.M.S. (mark.stevenson@crl.toshiba.co.uk).

LETTERS

Ultrafast superheating and melting of bulk ice

H. Iglev[1], M. Schmeisser[1], K. Simeonidis[1], A. Thaller[1] & A. Laubereau[1]

The superheating of a solid to a temperature beyond its melting point, without the solid actually melting, is a well-known phenomenon. It occurs with many substances[1–3], particularly those that can readily be produced as high-quality crystals. In principle, ice should also be amenable to superheating. But the complex three-dimensional network of hydrogen bonds that holds water molecules together and gives rise to unusual solid and liquid properties[4–11] strongly affects the melting behaviour of ice[12–14]; in particular, ice usually contains many defects owing to the directionality of its hydrogen bonds. However, simulations are readily able to 'create' defect-free ice that can be superheated[15,16]. Here we show that by exciting the OH stretching mode of water, it is possible to superheat ice. When using an ice sample at an initial temperature of 270 K, we observe an average temperature rise of 20 ± 2 K that persists over the monitored time interval of 250 ps without melting.

We have performed ultrafast temperature jump measurements in ice (for details on the experimental set-up and the sample preparation, see the Methods section) using the OH- and OD-stretching vibrations for rapid heating of the sample[17,18]. The same vibrational modes are known to be sensitive probes for H-bonding[19,20] and represent suitable spectral tools to distinguish local ice or water structures with a time resolution of a few picoseconds[20,21]. To illustrate this point, the steady-state infrared absorption spectrum of HDO:D_2O is shown in Fig. 1a for various temperature values. In the range 2,000–4,000 cm^{-1} the well-known OD- and OH-bands (left and right) occur with significant changes of position (blueshift) and shape with temperature. Figure 1b presents the same data as thermal differential spectra for $\Delta T = 20$ K. The spectrum corresponding to melting of the ice sample reduced by a factor of five is also shown in the Fig. 1b. The potential of the molecular vibrations as local probes of temperature and melting is readily seen.

Examples for the time-resolved differential spectra measured in a 2.5-μm-thick HDO:D_2O (15 M) ice specimen at 200 K are presented in Fig. 2. It shows ultrafast heating by two different processes: via infrared absorption of the OH- or the OD-stretching vibration. The transient spectra taken 50 ps after excitation are shown in Fig. 2a. The absorption changes are plotted for pump pulses of 3.0 μJ at 3,290 cm^{-1} (OH-pumping, blue points) and 2.7 μJ at 2,435 cm^{-1} (OD-pumping, red points). The adjustment of the pump-pulse energies ensures that approximately equal amounts of energy are deposited in the sample for both frequency settings. Both excitation schemes induce almost the same spectral changes in the HDO ice, indicating that the OH- and OD-oscillators are already at $t_D = 50$ ps in a local equilibrium. The similarity of the time-resolved data in Fig. 2a and the thermal differential spectra presented in Fig. 1b confirms induced heating of the sample. A comparison of the experimental data against differential spectra computed for various isochoric temperature jumps and the associated simultaneous pressure increase suggests an average temperature rise of 20 ± 2 K in the ice sample (Fig. 2b, see also the Methods section for further details). The isochoric pressure increase is estimated to be ~26 MPa.

The time evolution of the spectral changes induced by OH-pumping is depicted as a contour plot in Fig. 2c, showing that the frequency shift of the hydroxilic stretching modes—which appears as induced absorption in the high-frequency wings, indicated in red—has terminated after 20 ps. The temporal evolution of the spectral shift for both OH- and OD-pumping is documented by more quantitative data in Fig. 2d and e, for fixed probing frequencies of 2,435 cm^{-1} (OD probing, Fig. 2d) and 3,280 cm^{-1} (OH probing, Fig. 2e). At short delay times, fast signal changes occur at rates comparable to our time resolution under both excitation conditions, at both probing frequencies. (The signal overshoot for OH-pumping, shown by blue points in Fig. 2e at around $t_D = 0$ ps possibly involves a coherent pump-probe artefact in addition to depletion of the vibrational ground state.) For delay times longer than 20 ps, amplitude levels are constant. We can fit the data using a simple relaxation model with two assumed exponential time constants, and obtain a short relaxation time of $\tau_1 \leq 0.5$ ps consistent with the reported OH-lifetime of HDO ice[17,18] and a longer relaxation time of

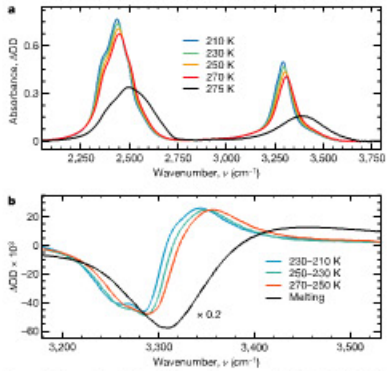

Figure 1 | Conventional infrared absorption spectra of HDO:D_2O (15 M). **a**, Absorption spectra of hexagonal ice in the OH- and OD-stretching region at various temperatures from 210 K (blue) to 270 K (red). The spectrum of the molten sample at 275 K (black line) is also shown. **b**, Same data as in **a** plotted as thermal differential spectra with $\Delta T = 20$ K. For a better view, the spectrum corresponding to melting of the ice sample is scaled by a factor of 0.2 (275–270 K, black line).

[1]Physik-Department, Technische Universität München, James-Franck-Strasse, D-85748 Garching, Germany.